Carderock Division
Naval Surface Warfare Center
West Bethesda, Maryland 20817-5700

NSWCCD-50-TR-2005 / 022 April 2005
Hydromechanics Department

Global Laser Rangefinder Profilometry (GLRP): A Novel Optical Surface-Wave Measurement System

by

Paisan Atsavapranee
Jason B. Carneal
Carl W. Baumann
John H. Hamilton
Jerry W. Shan

NSWCCD-50-TR-2005 / 022 Global Laser Rangefinder Profilometry (GLRP): A Novel Optical Surface-Wave Measurement System

REPORT DOCUMENTATION PAGE

Form Approved OMB No. 0704-0188

1. AGENCY USE ONLY (Leave blank)

2. REPORT DATE
March 2005

3. REPORT TYPE AND DATES COVERED
Final

4. TITLE AND SUBTITLE
Global Laser Rangefinder Profilometry (GLRP): A Novel Optical Surface-Wave Measurement System

5. FUNDING NUMBERS

6. AUTHOR(S)
Paisan Atsavapranee, Jason B. Carneal, Carl W. Baumann, John H. Hamilton, and Jerry W. Shan

7. PERFORMING ORGANIZATION NAME(S) AND ADDRESS(ES)
Carderock Division, Naval Surface Warfare Center
Code 5600
9500 MacArthur Boulevard
West Bethesda, Maryland 20817-5700

8. PERFORMING ORGANIZATION REPORT NUMBER
NSWCCD-50-TR-2005 / 022

9. SPONSORING / MONITORING AGENCY NAME(S) AND ADDRESS(ES)
Dr. L. Patrick Purtell
Office of Naval Research
800 North Quincy Street
Arlington, VA 22217-5660
703-696-4308

10. SPONSORING / MONITORING AGENCY REPORT NUMBER

11. SUPPLEMENTARY NOTES

12a. DISTRIBUTION / AVAILABILITY STATEMENT
Approved for public release: distribution unlimited.

12b. DISTRIBUTION CODE

13. ABSTRACT *(Maximum 200 words)*

Global Laser Rangefinder Profilometry (GLRP) is a novel optical technique for instantaneous planar measurement of complex three-dimensional surfaces. Even though its conception and development is driven primarily by the need to profile complex three-dimensional surface waves in naval hydrodynamic applications, the basic principle allows the extension of the technique to the measurement of solid surfaces as well. The working principle of GLRP is loosely based on that of a conventional laser rangefinder using triangulation. A triangulating laser rangefinder projects a beam of visible laser light to create a spot on a target surface. Scattered reflection from the surface is recorded at an angle by a line-scan detector, and the target distance is computed from the image pixel data. GLRP achieves comparable results but is able to perform cost-effective spatially distributed measurements at multiple locations over an entire surface. By utilizing multiple laser beams for tagging an array of points on the surface and recording the apparent positions of the laser spots with an area-scan CCD camera, the physical coordinates of the discrete points defining the target surface can be determined through calibration. In this paper, the basic working principle, along with the associated hardware and software algorithm for GLRP measurement are described. Data from a measurement of two-dimensional shallow-water waves using a prototype system with 100 measurement points are also presented and compared with flow visualization. Finally, an operational GLRP system designed and constructed for model-scale testing at NSWCCD is described, along with an estimate of the measurement uncertainty of the system.

14. SUBJECT TERMS
Global Laser Rangefinder Profilometry, surface wave, ship motion, wave dynamics, capsize

15. NUMBER OF PAGES
22+v

16. PRICE CODE

17. SECURITY CLASSIFICATION OF REPORT	18. SECURITY CLASSIFICATION OF THIS PAGE	19. SECURITY CLASSIFICATION OF ABSTRACT	20. LIMITATION OF ABSTRACT
Unclassified	Unclassified	Unclassified	Unclassified

THIS PAGE INTENTIONALLY LEFT BLANK

Contents

Figures

Tables

ABBREVIATIONS

AVI	Audio Video Interleave
CAD	computer-aided design
CCD	charge-coupled device
CFD	computational fluid dynamics
FWHM	full-width half-maximum
GLRP	Global Laser Rangefinder Profilometry
GUI	graphical user interface
MASK	Maneuvering and Seakeeping Basin
NSWCCD	Naval Surface Warfare Center, Carderock Division
OD	optical density
ONR	Office of Naval Research
PVC	polyvinyl chloride
RCM	radio-controlled model
RMS	root mean square
ROI	region of interest

ABSTRACT

Global Laser Rangefinder Profilometry (GLRP) is a novel optical technique for instantaneous planar measurement of complex three-dimensional surfaces. Even though its conception and development is driven primarily by the need to profile complex three-dimensional surface waves in naval hydrodynamic applications, the basic principle allows the extension of the technique to the measurement of solid surfaces as well. The working principle of GLRP is loosely based on that of a conventional laser rangefinder using triangulation. A triangulating laser rangefinder projects a beam of visible laser light to create a spot on a target surface. Scattered reflection from the surface is recorded at an angle by a line-scan detector, and the target distance is computed from the image pixel data. GLRP achieves comparable results but is able to perform cost-effective spatially distributed measurements at multiple locations over an entire surface. By utilizing multiple laser beams for tagging an array of points on the surface and recording the apparent positions of the laser spots with an area-scan CCD camera, the physical coordinates of the discrete points defining the target surface can be determined through calibration. In this paper, the basic working principle, along with the associated hardware and software algorithm for GLRP measurement are described. Data from a measurement of two-dimensional shallow-water waves using a prototype system with 100 measurement points are also presented and compared with flow visualization. Finally, an operational GLRP system designed and constructed for model-scale testing at NSWCCD is described, along with an estimate of the measurement uncertainty of the system.

ADMINISTRATIVE INFORMATION

This work was performed at the Naval Surface Warfare Center, Carderock Division and was sponsored by ONR WRN: N0001405-WX-20487, under the direction of Dr. L. Patrick Purtell of the Office of Naval Research (Code 333). The Project Leader at the Naval Surface Warfare Center, Carderock Division was Dr. Paisan Atsavapranee of the Maneuvering and Control Division (Code 5600).

INTRODUCTION

Experimental measurement of surface-wave elevation plays an important role in many free-surface flow studies of both fundamental and practical interests. With the increasing use of computational tools in connection with complex nonlinear wave dynamics around surface vessels in deep-ocean and coastal regions, time-resolved three-dimensional surface-wave data have become even more crucial in model development and in the validation of flow solutions. For instance, wave-induced motions of a surface

ship in severe weather can cause passenger discomfort, large hull loads, cargo damage, and even capsize. Current ship motions prediction programs consider various components of external forces, including hydrostatic restoring and Froude-Krylov wave forces, radiation and diffraction forces, viscous roll damping, and appendage forces from propellers, bilge keels, rudders and fins. Usually each of the components of forces is computed separately and linearly superposed to yield total forces and moments. In cases where nonlinear wave interactions are significant, experimental data on the wave field around the ship and the associated six-degree-of-freedom ship motions are necessary to develop more sophisticated models and to validate predictions. The problem becomes even more complex with the consideration of multi-hull designs where wave-making interaction of various waterplane sections can play a significant role in resistance and seakeeping.

Model testing at various tow-tank organizations employs many measurement techniques such as sonic and electro-mechanical devices to measure surface wave elevation at a few discrete locations. One example of these devices is the "whisker probe," which uses a stainless steel needle or whisker mounted on a support arm to probe the surface of the water by electrical conductivity. Upon entry of the whisker into the water, the small electrical potential on the whisker is grounded out, and a positional readout proportional to the water level is output. The probe then begins retracting the whisker out of the water until the meniscus on the needle tip breaks, at which point the whisker is again lowered into the water to begin another cycle. By keeping the whisker arm very light, data rates of 60 measurement cycles per second have been achieved, although operation in the 30 to 40 Hz range is more practical.

The use of electro-mechanical devices such as the whisker probe has thus far been mostly limited to the measurement of steady wave profiles for two reasons. Firstly, the mechanical design of the whisker probe does not allow the measurement of large peak-to-peak waves. Secondly, it is impractical to employ more than a few electro-mechanical devices simultaneously in an experiment. For many seakeeping and maneuvering problems, particularly those involving large-amplitude waves and ship motions, it is necessary to obtain dynamic measurement of the three-dimensional wave surface at a large array of points around a ship model.

Currently few techniques exist that would allow the measurement of complex three-dimensional surface of water waves. These concepts include the measurement of surface slope by intensity-based reflection[1], color-encoded optical reflection[2] and light shadowgraphy[3]. These techniques, however, are limited to the measurement of small wave slope over a small physical area. To date none of these techniques is suitable for practical large-scale surface wave measurements in tow-tank facilities. GLRP was conceived and designed with such needs in mind, providing high-rate three-dimensional mapping of surface waves over a large physical area, making it suitable for the study of large-amplitude transient wave dynamics in large-scale facilities. With further development, it is conceivable that the use of GLRP can be extended to full-scale trials for the use of profiling surface waves in the near field of ocean-going vessels.

DESCRIPTION AND OPERATION OF GLRP

At the most fundamental level, Global Laser Rangefinder Profilometry operates in a similar way to a conventional laser rangefinder based on triangulation. A triangulating laser rangefinder projects a beam

of visible laser light that creates a spot on the target surface. For diffuse surfaces, scattered reflection is viewed from an angle by a line-scan detector through a collection lens. The apparent position of the spot image on the pixel elements of the line-scan detector changes with the viewing angle and the distance to the target, and thus the distance to the target can be computed from the image pixel data. Figure 1 shows a diagram illustrating the working principle of a laser rangefinder using triangulation. Usually, commercial laser rangefinders using triangulation are designed for measurements with short standoff distances, but measurement resolution can be very high, approaching 0.01% of full-scale span in some instances.

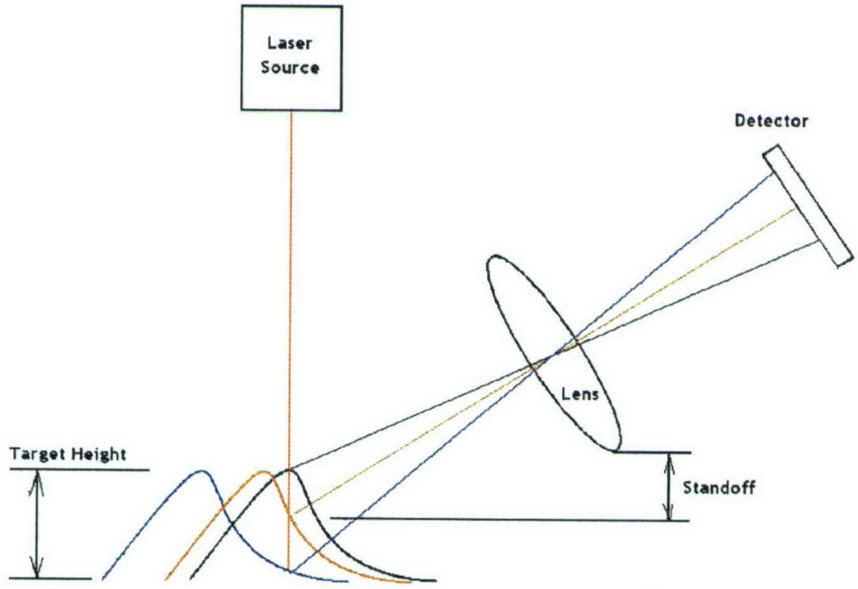

Figure 1: A schematic illustrating the working principles of a triangulating laser rangefinder.

GLRP Working Principle

GLRP extends the concept of a triangulating laser rangefinder from a single-spot measurement to a cost-effective, spatially-distributed measurement at a large number of points over a three-dimensional surface of interest. The technique utilizes multiple laser beams from inexpensive commercial-off-the-shelf laser diodes for tagging discrete points on the surface and recording the apparent positions of the laser spots with an area-scan CCD camera. The physical coordinates of the measurement points defining the target surface can then be determined through calibration. The main feature of GLRP measurement is the fact that a typical mega-pixel CCD camera operating at video rate can easily record the positions of hundreds of laser spots simultaneously, allowing the dynamic profiling of a surface whose deformation changes rapidly in time. Only a single camera is necessary, simplifying the experimental setup and reducing hardware and operating cost. Since GLRP is an optical non-intrusive measurement, it is also highly adaptable and scalable to many scientific and industrial applications.

Laser Diode Array and Camera

Figure 2 illustrates the experimental setup for a GLRP prototype system used to profile two-dimensional shallow-water waves in the Miniature Water Basin at the Naval Surface Warfare Center, Carderock Division (NSWCCD). A basic GLRP setup is comprised of an array of laser diodes used to illuminate the surface of interest and a progressive-scan CCD camera to record the images of the laser spots. The 60-cm x 60-cm diode panel is constructed of a 12.5 mm-thick sheet of PVC with 100 mounting holes drilled perpendicular to the panel on a 50.8-mm x 50.8-mm grid. A laser diode operating at 650 nm with a typical output of 3.5 mW is installed into each mounting hole, without any special provision for alignment. The entire panel is then rotated 5 degrees from horizontal, so that all 100 laser beams make an approximately 5-degree slant angle to the water surface. A single CCD camera (Roper Scientific ES4.0), operating at 30 fps and 1024 x 1024 pixel resolution, is mounted next to the panel at a small angle, so that field of view covers the images of all the laser spots over the full range of water elevation.

Laser Spot Images

In order to mark the surface of the water with laser spots, an aqueous solution of Oxazine 725 chloride dye (10^{-4} molarity) is sprayed onto the surface of the water before each measurement. Oxazine 725 chloride has a strong absorption peak around the laser wavelength and fluoresces brightly with laser illumination. For high enough concentrations, most of the laser energy is either reflected or absorbed at the surface, with little of the laser beam energy penetrating the surface. An interference filter with a peak transmission of 50% at 700 nm and a FWHM of 40 nm with a blocking OD of 4.0 is fitted on the camera lens to attenuate the reflected beam and ensure that only diffuse fluorescent light from the water surface is recorded. In such a way, the apparent positions of the laser spots recorded by the camera correspond to the physical intersection of the laser beams with the water surface.

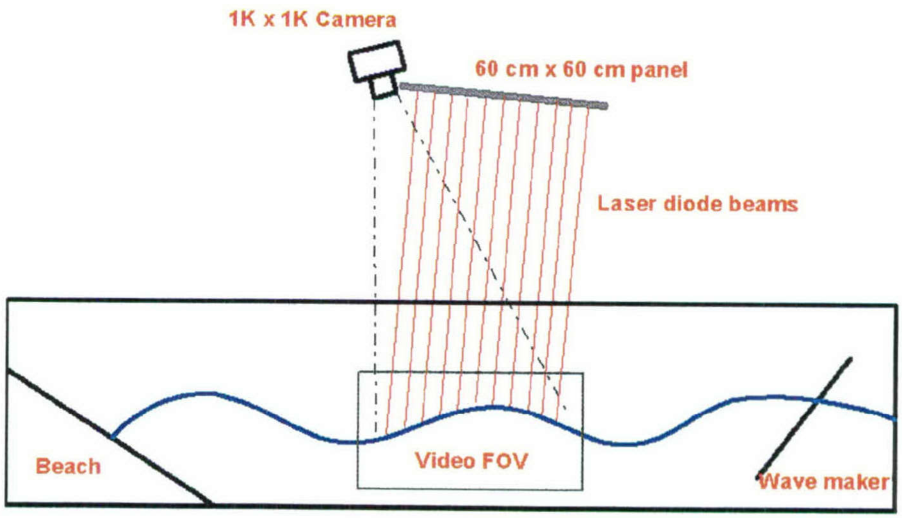

Figure 2: GLRP prototype at the Miniature Water Basin at NSWCCD. 100 laser diodes are distributed on a 50.8 mm square grid.

Figure 3 shows a superposition of five images of the laser spots, taken in calm water at 35.56 cm, 38.10 cm, and 40.64 cm, 43.18 cm, and 45.72 cm water elevations. It is clear that the apparent positions or pixel locations of the laser spots on the CCD array change with the water elevation. A change in the water elevation causes a real spatial displacement in the intersection points of the laser beams to the water surface, both vertically and laterally. When viewed from top, the physical lateral displacement of the laser spots causes a corresponding shift in the spot images on the CCD array. Also, the physical vertical displacement causes a local change in the magnification ratio of the imaged spots, resulting in an apparent shift of the spots when viewed off-axis from the camera optical axis. The relative contribution of these two effects to the positional shift of the laser spots in the image plane depends primarily upon the ratio of the peak-to-peak wave elevation under investigation and the distance from the camera to the surface (standoff distance). For example, if the camera is sufficiently far away, there would be little change in the local magnification of the laser spots as the water elevation changes, and the shift in the pixel locations of the laser spots would be due primarily to the beam angle. By determining the pixel location of each laser spot from images recorded during an experiment, the surface elevation at each of the measurement points can be determined as a function of time through calibration.

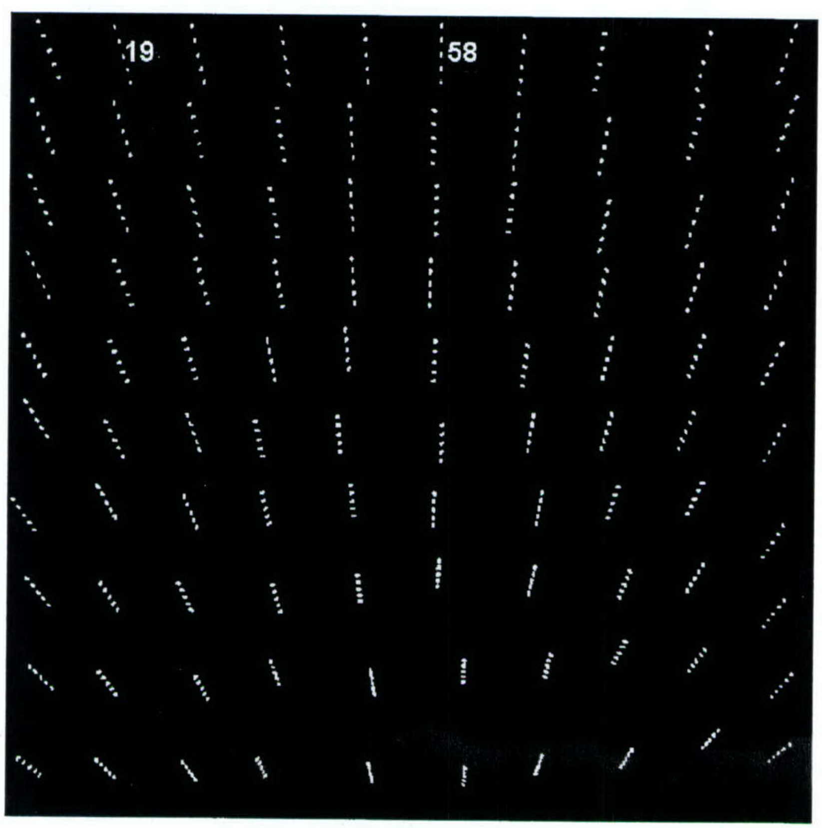

Figure 3: A superposition of five surface displacement calibration images of the laser spots, taken in calm water with 35.56 cm, 38.10 cm, and 40.64 cm, 43.18 cm, and 45.72 cm water elevations.

Calibration Procedure

It is possible to write in analytical form the relationship between the shift in the pixel locations of the laser spots in the image plane and the changes in surface elevation at each of the measurement locations. However in practice, an attempt to measure surface elevation in such a way is prone to significant error, because it requires precise knowledge of the optical transfer function of the imaging system and the origin and angle of each laser beam. Instead, a calibration procedure is prescribed that allows the relationship between the local surface elevation and the apparent position of each laser spot to be determined in an empirical manner. Two separate static calibrations are required in order to accurately determine the physical coordinates (x_p, y_p, z_p) of the laser spots from the apparent or pixel coordinates (x_a, y_a) in the image pixel data. The surface displacement calibration yields the relationship between z_p and (x_a, y_a), and the X-Y mapping calibration yields the relationship between (x_p, y_p) and (x_a, y_a).

Surface Displacement Calibration

The first portion of the static calibration procedure involves recording an image of the laser spots in calm water at different surface elevations in the experimental facility. For a small-scale facility, changing the water level can be easily accomplished by adding or removing water until the water surface reaches the desired elevation. For a large-scale facility in which changing the water level is impractical due to the large volume of water, the laser diode panel and the camera can be mounted together and lowered or raised as one unit to simulate the incremental change in surface elevation. For the experiment described in Section 3, the surface displacement calibration images at five different surface elevations are shown superposed in Figure 3. Once the set of calibration images is obtained, surface displacement calibration curves for the laser diodes are constructed from the pixel coordinates of the laser spots at each surface elevation, as explained in detail in Section 2.4.1.

X-Y Mapping Calibration

In addition to the surface displacement calibration which yields the calibration curves for the vertical coordinate z_p of the measured surface, it is also necessary to obtain the calibration curves for the lateral coordinates (x_p, y_p) by X-Y mapping calibration. This part of the static calibration procedure involves recording an image of a calibration target placed at several standoff distances from the imaging system. The front face of the calibration target contains markers, crosses or dots painted onto the target in a regular grid pattern. Figure 6(a) illustrates an image, viewed from a slant angle, of a 60-cm square calibration target with cross markers in a 50.8-mm x 50.8-mm regular grid pattern. Usually, it is practical but not necessary, to place the front face of the target in the same planes as the different surface elevations chosen in the surface displacement calibration. Again, either the target itself can be lowered or raised or the laser diode panel and the camera can be mounted together and lowered or raised as one unit to simulate the incremental change in the standoff distance. Once the set of X-Y mapping calibration images is obtained, X-Y mapping calibration curves for the laser diodes are constructed from the pixel coordinates of the markers at each surface elevation, as explained in detail in Section 2.4.1

Data Processing

Once the calibration curves have been obtained through the procedures outlined in Section 2.2, the test data, comprised of a sequence of images obtained during an experimental run are now ready to be processed. In practice, the data processing procedure consists of four separate steps (preprocessing, blob analysis, coordinate mapping, and postprocessing). Each image is first multiplied by a region-of-interest (ROI) mask (preprocessing) created using the surface displacement calibration images (see Figure 7). This step ensures that any noise outside the expected path of the laser spots are cancelled out before blob analysis is performed. Next, blob analysis is performed to identify the discrete laser spots and determine their centroids. All the identified laser spots are then assigned an index number, which provides each laser spot an association to a physical laser diode. The calibration curves are then applied to the centroid pixel coordinates for each laser spot to determine the physical coordinates (x_p, y_p, z_p) of the wave surface (coordinate mapping). And finally, a set of criteria is applied to each of the identified laser spots to discard outliers (postprocessing). Details of the separate steps in the data processing procedure are provided in the description of the GLRP software package in Section 2.4.

The GLRP Software Package

A GLRP software package has been developed in-house at NSWCCD. A flow-chart of the developed software is shown in Figure 4. The program core algorithms include a calibration module and a data processing module, controlled by a graphical user interface (GUI). The GUI provides dynamic control of the GLRP process, allowing the user to load and save user settings, perform multiple calibrations, and specify the variables used in the performance of calibration and data processing. In addition, the GUI gives the user the ability to specify several output types including AVI movies and text data files. The GUI serves as a main program, while the calibration and data processing modules act as functions within the main program.

Calibration Module

The calibration algorithm is crucial to the accurate determination of a surface wave profile. The calibration module performs both surface displacement calibration and X-Y mapping calibration in the GLRP software package, by taking user inputs as arguments and providing an ROI mask image, a diode-index mask image, and calibration curves for each of the physical laser diodes as outputs to the other modules in the software package.

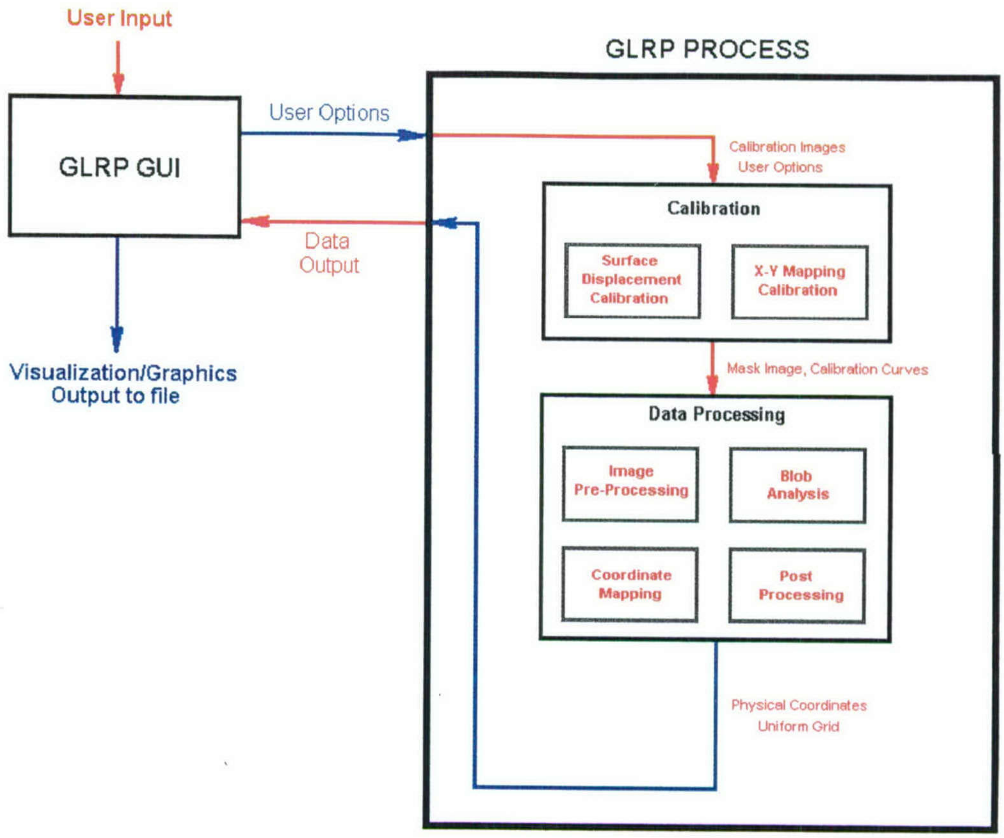

Figure 4: GLRP software package block diagram, illustrating the different functional modules.

Surface Displacement Calibration Algorithm

The surface displacement calibration algorithm takes several user inputs, including the number of calibration images N, the surface elevation corresponding to each calibration image, a search radius for corresponding diode locations in successive images, and an allowed path deviation radius. The calibration images are processed with the blob analysis algorithm (see Section 2.4.2) to determine the pixel coordinates of the laser spots, using an intensity-weighted centroid estimation algorithm. In order to associate the laser spots to specific laser diodes, the initial image taken at a neutral water elevation is processed first to obtain the centroid pixel location for each laser spot in the image. Each detected laser spot image is then assigned a unique diode-index number. As subsequent images are processed, detected laser spots are labeled according to a nearest neighbor search from the list of centroids detected in the previous image. The radius of the nearest neighbor search is controlled by the user-defined search radius. This process is repeated in order to build an (x_a, y_a) coordinate history at every calibration height for each laser diode. Finally, this coordinate history is used to construct the ROI mask image, the diode-index mask image, and calibration curves for each laser spot.

Each physical laser diode is now associated with an (x_a, y_a) coordinate history, comprising N pixel coordinates of its image centroids at successive water elevations. A new independent variable R is then calculated from the (x_a, y_a) coordinate history:

$$R = \left[(x_a - x_o)^2 + (y_a - y_o)^2\right]^{\frac{1}{2}} \quad , \tag{1}$$

where x_o and y_o are the coordinates of the image centroid at the neutral water elevation. Using user-defined calibration heights for each calibration image as the dependent variable z_p, a surface displacement calibration curve can now be plotted for each of the laser spots using a second-order polynomial least-squares fit:

$$z_p = a_0 + a_1 R + a_2 R^2 \tag{2}$$

The z_p calibration curves for all physical laser diodes are then saved for use by the data processing module. Some examples of surface displacement calibration curves are presented in Figure 5. The two curves shown correspond to the two groups of laser spots in Figure 3 marked with indices 19 and 58.

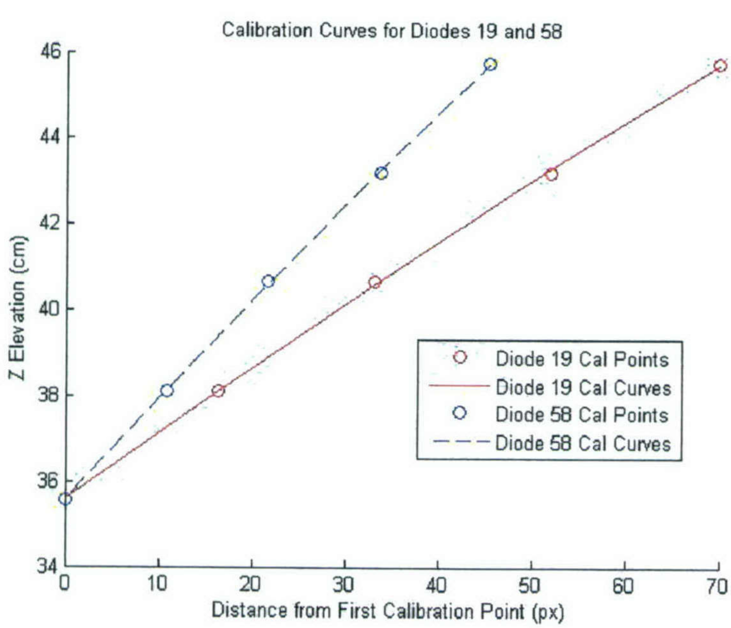

Figure 5: Example calibration curves from surface displacement calibration. See Figure 3 for corresponding groups of laser spot images.

X-Y Mapping Calibration Algorithm

The X-Y mapping calibration algorithm provides the calibration curves for the calculation of the physical coordinates (x_p, y_p) from the (x_a, y_a) coordinates in the image plane. For each image, a geometrical transform that would "dewarp" the marker locations in the original calibration image into a regular grid pattern is performed (see Figure 6), yielding a set of coefficients that describes the mapping function between the image and physical coordinate systems. First, each image is processed using an adaptive histogram equalization, a boundary subtraction, and a nonuniform background illumination correction in order to eliminate false marker detections. The images are then converted to binary format using a histogram threshold. The markers are detected and identified using a 4-connected search algorithm, and a centroid estimation is performed using an unweighted centroid estimation technique. These estimated centroid locations of the markers are then used as starting points in a refined step to locate the centroid for each marker by performing cross-correlation of the local image intensity with a template image of a synthetic marker with Gaussian intensity distribution.

In order to dewarp the image into a uniform grid, the detected markers are sorted into rows and columns. Each marker is assumed to be on a regular grid in the dewarped image, and pixel coordinates in the dewarped image for each marker are calculated. The refined centroid and dewarped coordinates of each marker are then used to determine the coefficients of a projective transform between the calibration image plane and the dewarped image plane. The user is then prompted to select the center marker in the original image to provide a reference location in the transformed space. Given user-defined physical coordinates of the reference marker and physical spacing between the markers, the physical transform is determined using the known reference position and the pixel coordinates of each marker in the dewarped image.

Next, the pixel coordinates of the laser spot centroids obtained from the surface displacement calibration algorithm are tranformed using the appropriate set of mapping coefficients into *x-y* physical coordinates (x_p, y_p). Using the coordinates x_p and y_p now as the dependent variables, the lateral coordinates of the water surface at each measurement point can now be expressed, using a second-order polynomial least-squares fit, as functions of the independent variable R:

$$x_p = b_0 + b_1 R + b_2 R^2 \tag{3}$$

and

$$y_p = c_0 + c_1 R + c_2 R^2 \ . \tag{4}$$

The two X-Y mapping calibration curves for each diode are then saved for use by the data processing module.

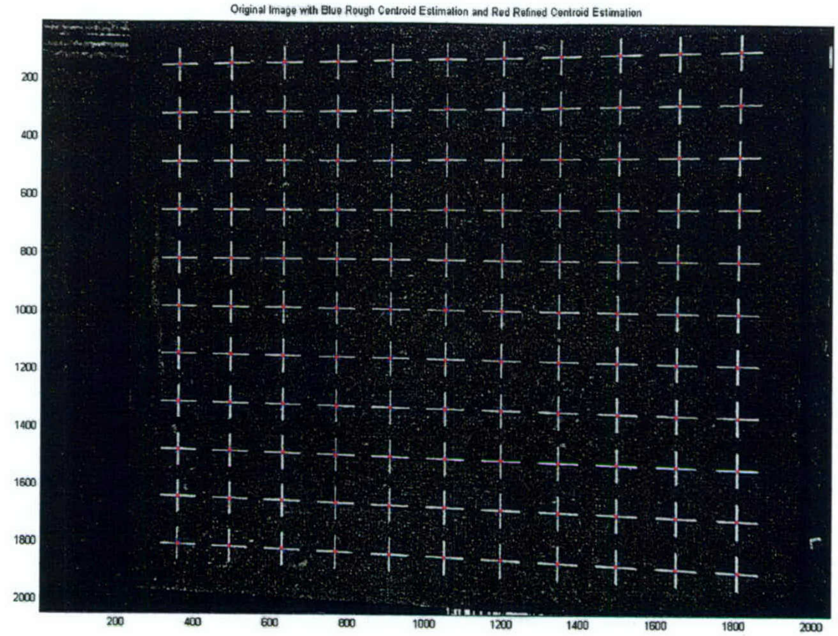

a)

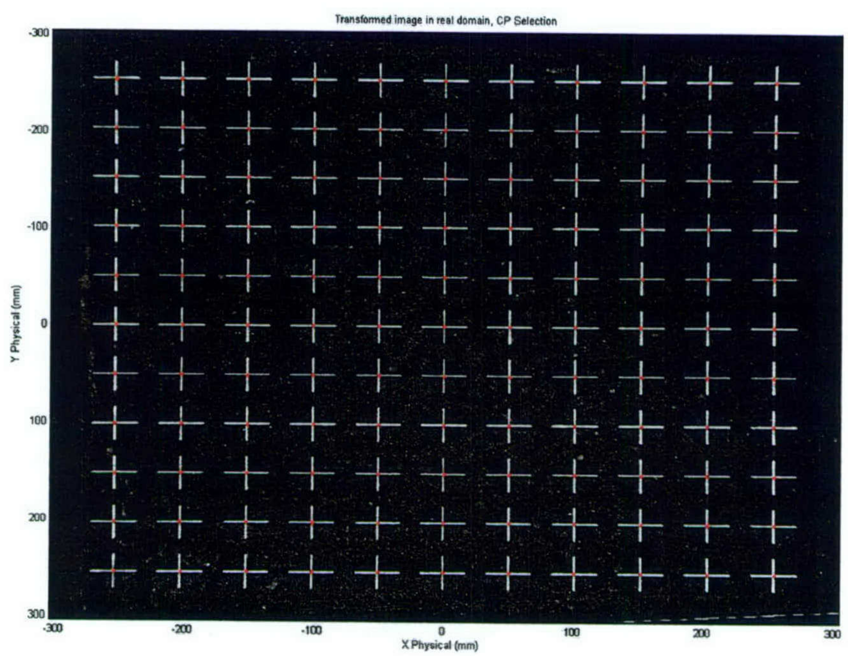

b)

Figure 6: Image of calibration target recorded at a slant angle (a) and after mapping of the markers onto a regular grid (b). Red dots in images denote the centers of the markers found by the detection algorithm.

ROI Mask and Diode-index Mask

In order to create an ROI mask image, a line is drawn between each successive (x_a, y_a) coordinate pair assigned to a particular diode in the coordinate history from the surface displacement calibration. Any pixel within the user-defined allowed path deviation radius of the resulting lines is assigned a value of 1, while all other pixels in the ROI mask image are set to a value of 0. This process is repeated for each identified diode. A sample ROI mask image is shown in Figure 7. The constructed image contains a region of interest (ROI) for each diode in which detected laser spots are considered as valid.

The diode-index mask image is created in a similar way as the ROI mask image, except that any pixel within the user-defined allowed path deviation radius is assigned a value equal to the diode-index number. In such a way, the diode-index number is stored in each diode ROI and can be easily accessed by other modules in the software package.

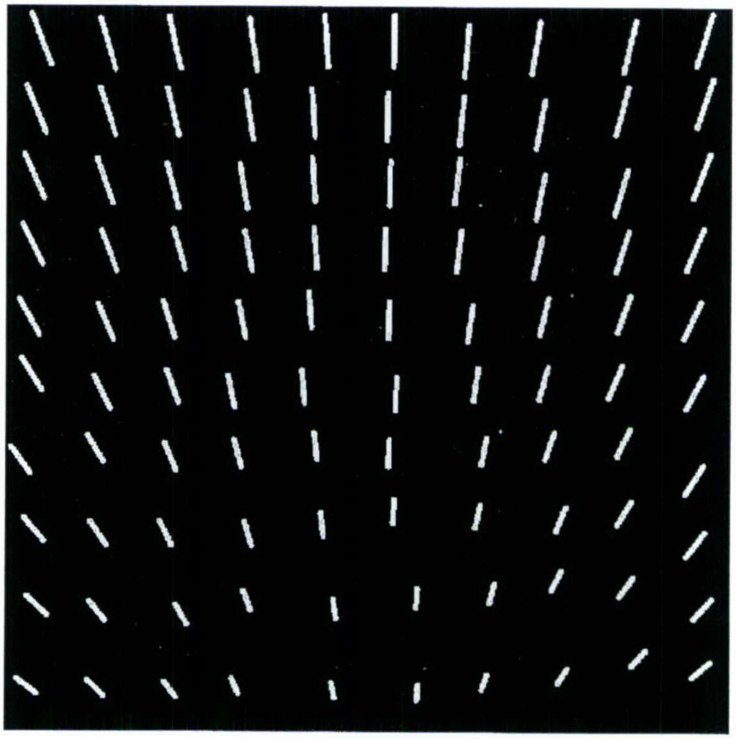

Figure 7: ROI mask image from the Miniature Water Basin demonstration experiment, using search radius of 20 pixels and allowed path deviation radius of 4 pixels.

Data Processing Module

The data processing module performs several functions on the images recorded during an experiment. The main functions included in the data processing module are image pre-processing, blob analysis, coordinate mapping, and post-processing. These functions ultimately take user inputs and calibration information and output the profile of the wave surface.

Image Pre-Processing

The image pre-processing function involves multiplying the raw images captured during the data collection procedure with the ROI mask image. The ROI masking process eliminates the detection of particles outside of the diode regions of interest, and reduces false detection of other phenomena such as specular reflection and noise.

Blob Analysis

After the images are pre-processed, blob analysis is performed on the resulting images. Each contiguous region of pixels with high intensity are grouped together and assigned a diode-index number. Each group's centroid is calculated using an intensity-weighted centroid estimation scheme. Sample results from the blob analysis module from a raw image obtained with the MASK GLRP system (see Section 4) are shown in Figure 8. In order to associate the detected centroid with a particular physical diode for coordinate mapping, the centroid coordinate values are rounded off and the diode-index mask is accessed at that pixel location to determine the diode-index number for the detected laser spot.

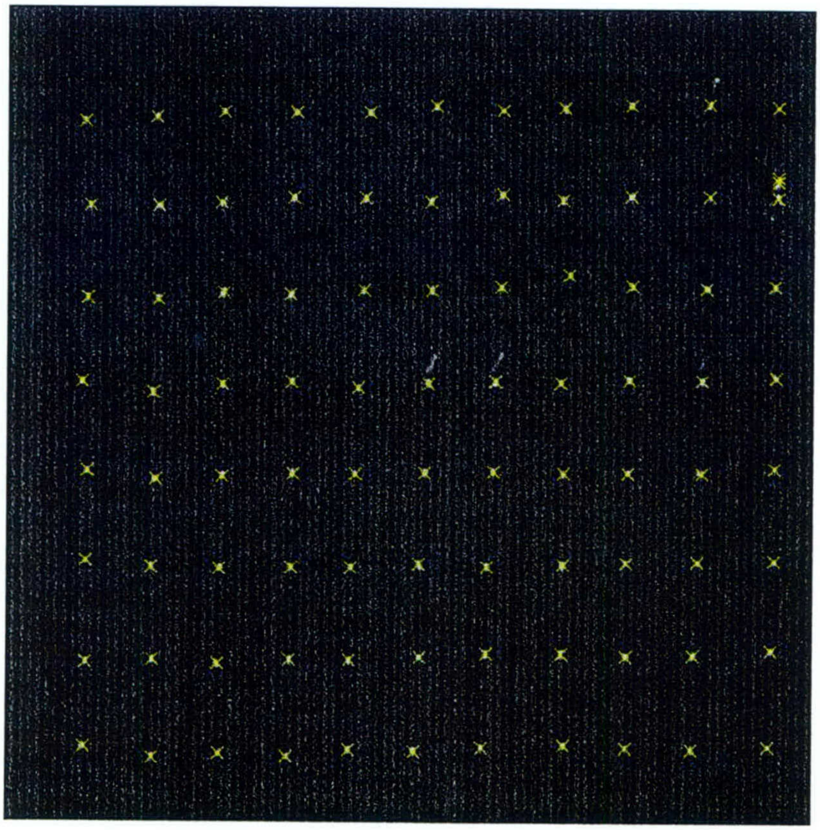

Figure 8: Sample results from the blob analysis algorithm using a raw image obtained with the MASK GLRP system. The crosses mark the blob centroids detected by the centroid estimation scheme.

Coordinate Mapping

Once the diode locations in each image have been identified, each centroid coordinate is assigned a specific diode-index number, and the distance quantity R is determined for the detected laser spot using equation (1). Coordinate mapping is then performed by using the calibration curves for (x_p, y_p, z_p), as shown in equations (2)-(4), to calculate the physical location of the water surface in three dimensions.

Post-Processing

The output of the coordinate mapping function yields multiple physical coordinates corresponding to the intersection of laser beams with the water surface. A post-processing function performs the elimination of spurious data points on the measured wave surface and the interpolation of the data to a regular grid. A 3x3 validation scheme is used to eliminate spurious data points in the GLRP output. For each point, the average and RMS values of the neighboring 8 points are calculated. If the value of the center point differs from the average value by more than a user-specified multiple of the RMS value, the data point is removed from the data set. Additionally a particle tracking algorithm, which utilizes *a priori* information from the previous frame, may also be used to determine an expected location for the laser spot in the current frame. If the detected laser spot does not fall within a given search radius of the expected position, the laser spot is disregarded.

If interpolation is selected, a surface is fitted through the physical locations using a triangle-based linear interpolation scheme. Higher-order fits will be included in future versions of the software. The interpolation module provides (x_r, y_r, z_r) on a uniform grid, which will be advantageous in comparison to computational fluid dynamics (CFD) calculations and other analytical methods

RESULTS FROM DEMONSTRATION EXPERIMENT

The GLRP prototype system described in Section 2.1.1 was used to profile two-dimensional shallow-water waves in the Miniature Water Basin at NSWCCD for purposes of concept demonstration and development. The Miniature Water Basin is a 15-m long x 0.6-m wide x 0.7-m deep water basin with a paddle-type wavemaker on one end and a beach at the other. A two-dimensional wave train was generated by the 0.6-m x 0.6-m wavemaker, with the waves traveling from right to left, and GLRP measurement was performed roughly in the middle of the basin. A total of 100 laser diodes were used to profile the wave surface over an area 0.5 m x 0.5 m in size, at a rate of 30 fps. Flow visualization through the clear sidewall of the basin was also performed using a video camera and provides a qualitative comparison to the measurement next to the sidewall.

In this demonstration experiment, only the surface displacement calibration was performed. This step yields a set of calibration images as shown superposed in Figure 3 and a set of surface displacement calibration curves for each of the laser spots. Since no X-Y mapping was obtained, a simple uniform conversion of the pixel coordinates of the laser spots to physical coordinates (using scale from a ruler) was performed for the calibration image taken at 35.56 cm water elevation. Lateral shift of the laser spots at a different water elevation can then be calculated assuming uniform beam angle of 5 degrees. Using such estimate for (x_p, y_p) and a calculation of z_p using surface displacement calibration curves, a cloud of dots representing the water surface can be plotted in three-dimensions at successive time steps. A short time sequence of the surface data taken every 1/30 second is shown in Figure 9.

During the setup of this demonstration experiment, the edge of the GLRP measurement area was intentionally placed as close as possible to the sidewall through which the flow visualization video were to be taken. The GLRP data along the line closest to the sidewall (represented by red circles) was then superimposed upon the flow visualization pictures of the waves to provide a qualitative comparison and validation of the technique. Figure 10 presents a short time sequence of the overlaid images. The time points of each video frame in Figure 10 corresponds to the same time as the corresponding frame in the set of 3D plots of the GLRP data in Figure 9.

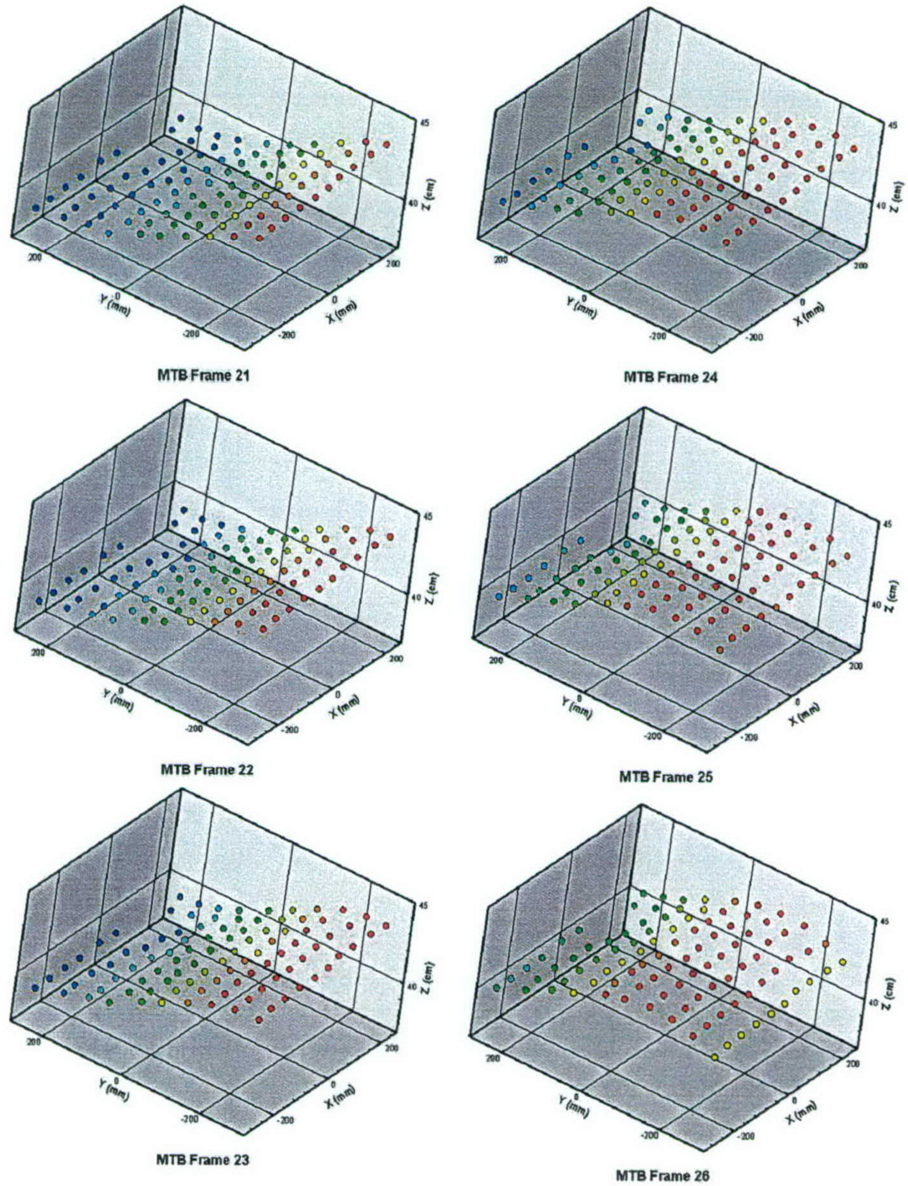

Figure 9: A short time sequence of the three-dimensional surface data taken at 30 Hz.

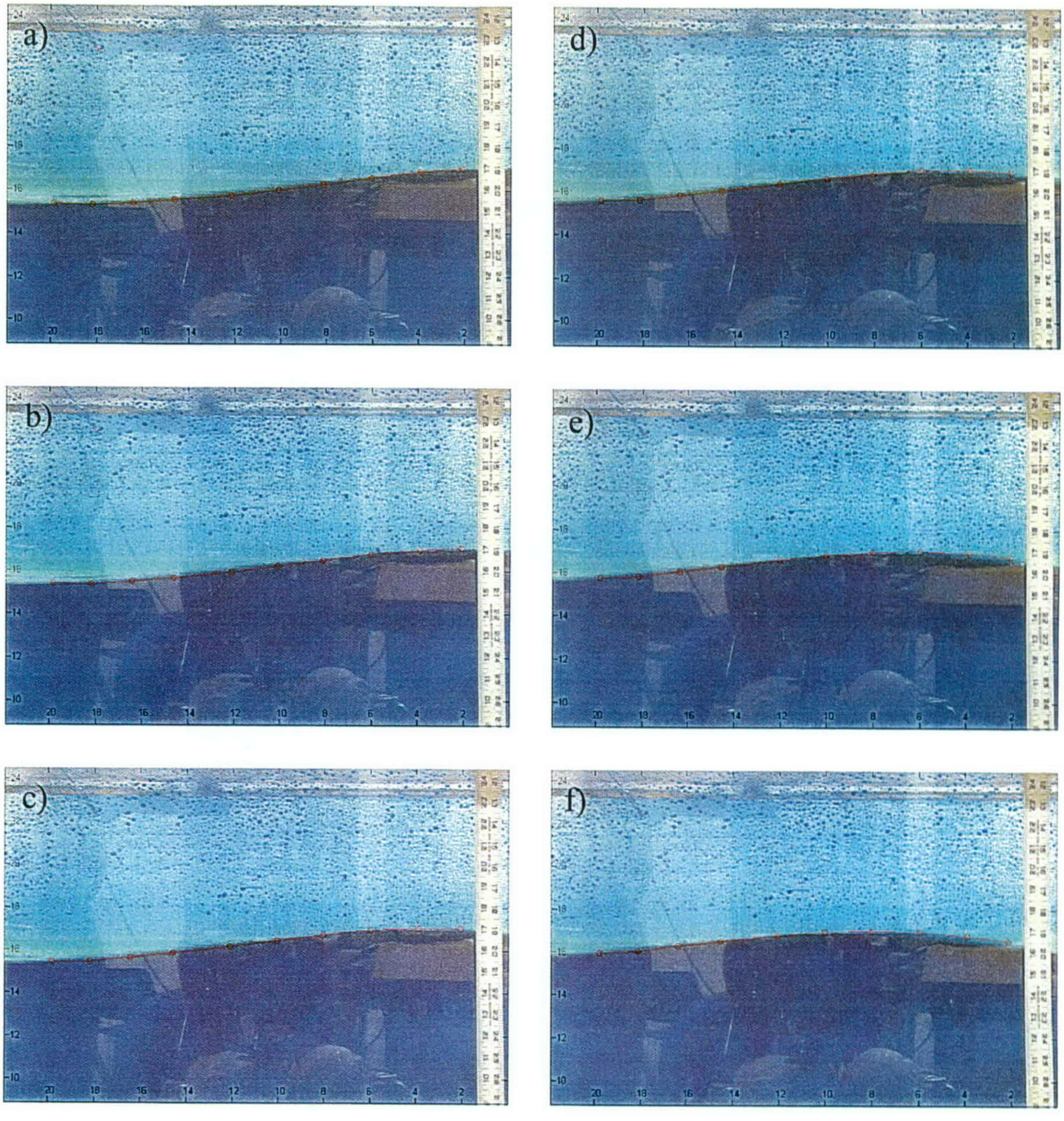

Figure 10: A sequence of video stills showing the side view of the water waves. GLRP data (red circles) taken close to the sidewall are superposed showing excellent comparison.

THE MASK GLRP SYSTEM

An operational GLRP measurement system was designed and constructed for surface wave measurement in the Maneuvering and Seakeeping Basin (MASK) at NSWCCD. The basin is approximately 110 m long x 73 m wide x 6.1 m deep. As illustrated in Figure 11, the basin is spanned lengthwise by a 114.6 m bridge supported on a rail system that permits the bridge to traverse one-half the width of the basin and to rotate through angles up to 45 degrees from the longitudinal centerline of the basin. Ship models can be towed in head or following seas at any angle from 0 to 90 degrees. Tracks attached to the bottom of the bridge support the towing carriage, 6.1 m wide, 6.6 m long, and 2 m high with a maximum speed of 7.7 m/s. Eight pneumatic wavemaker units are located along one 73 m side of the basin and 13 units along one 110 m side. They can be operated in unison or individually, permitting regular wave generation up to 0.6 m in height and irregular wave generation simulating the ocean up to a scaled sea state 9.

The MASK GLRP system was designed to be suitable for general model-scale testing, including maneuvering experiments with free-running models, dynamic stability and capsizing experiments, and ocean engineering experiments for floating, moored, and fixed structures. A 6.4 m long x 4.7 m wide support platform (Figure 12) was installed off the side of the MASK bridge around the midspan. The platform houses four measurement panels (Figure 13), each mounted to a linear traversing system with a vertical travel of 0.6 m. Each panel is 0.76 m x 1.52 m in size and holds 200 laser diodes (655 nm, 25 mW output), installed every 7.6 cm in a regular grid pattern.

Each panel utilizes two progressive-scan CCD cameras (Hitachi model #KP-F120CL) operating at 1392 x 1040 pixel resolution and a repetition rate of 30 fps, each recording the images of 100 laser spots. The cameras are hard-mounted to the laser diode panels so they can be lowered or raised as one unit for calibration purposes. The four measurement panels and eight cameras used together can profile the water surface at 800 discrete measurement points, with a repetition rate of 30 Hz over an area roughly 1.6 m x 3.2 m in size. The images from the eight CCD cameras are acquired and stored onto two acquisition computer systems, each capable of recording images from four cameras simultaneously. Each computer system utilizes a high-capacity real-time disk system that allows continuous recording of the images from all four cameras at the full frame rate.

A sprinkler system installed around the platform allows the Oxazine 725 dye solution to be sprayed onto the surface of the water before each measurement run. Eventually the dye disperses over time, but continuous measurement over 1-2 min period can be readily achieved. Once the dye disperses, the laser beams no longer make distinct spots on the surface, resulting in a degradation of the measurement. The length of a typical experimental run performed in the MASK falls under the 1-2 min range, allowing the continuous measurement of dynamic events in most cases.

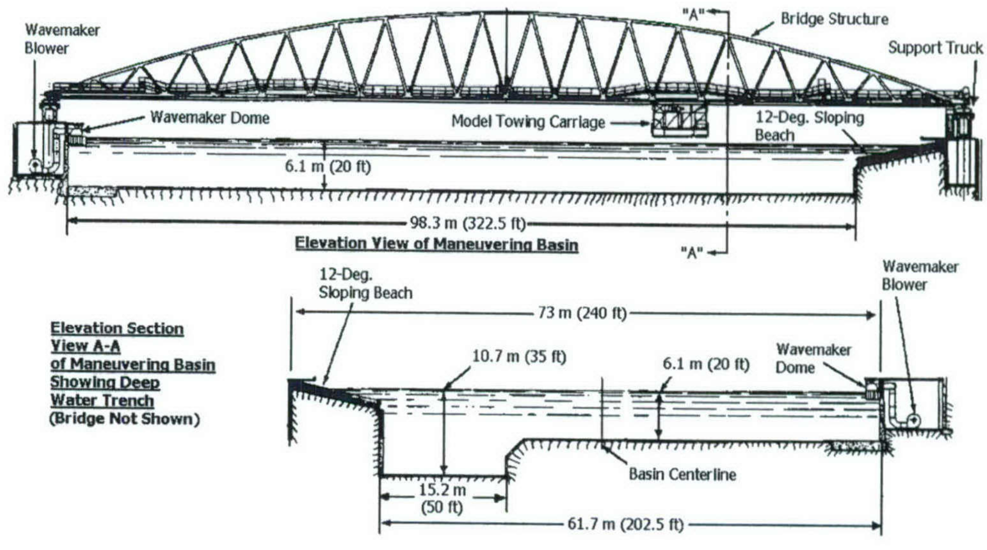

Figure 11: Elevation view of Maneuvering and Seakeeping Basin at NSWCCD.

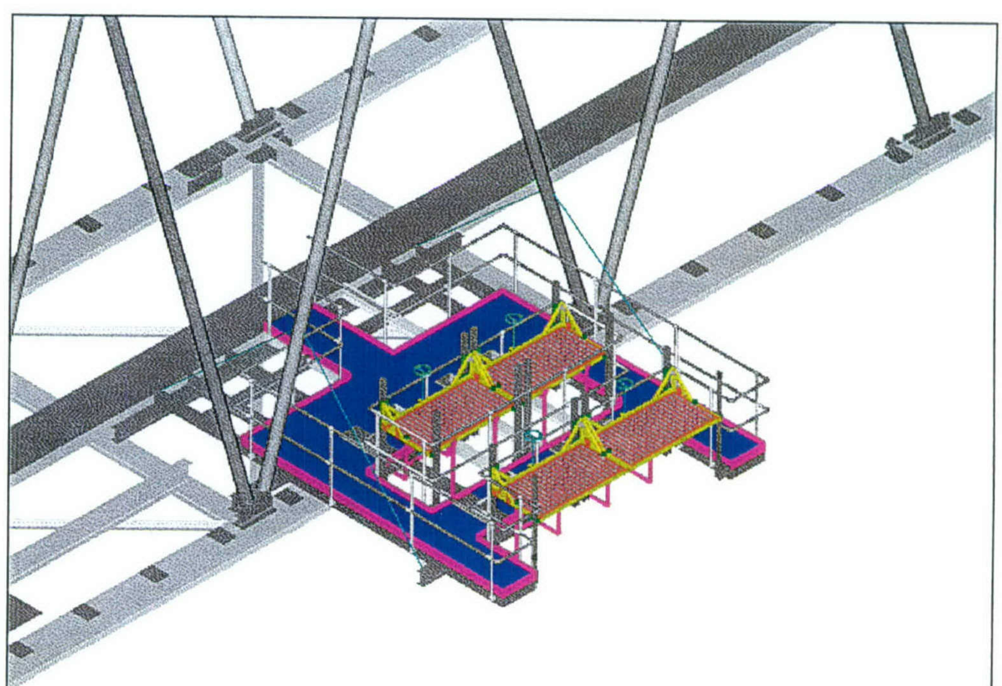

Figure 12: A CAD rendering of the GLRP system off the side of the MASK bridge.

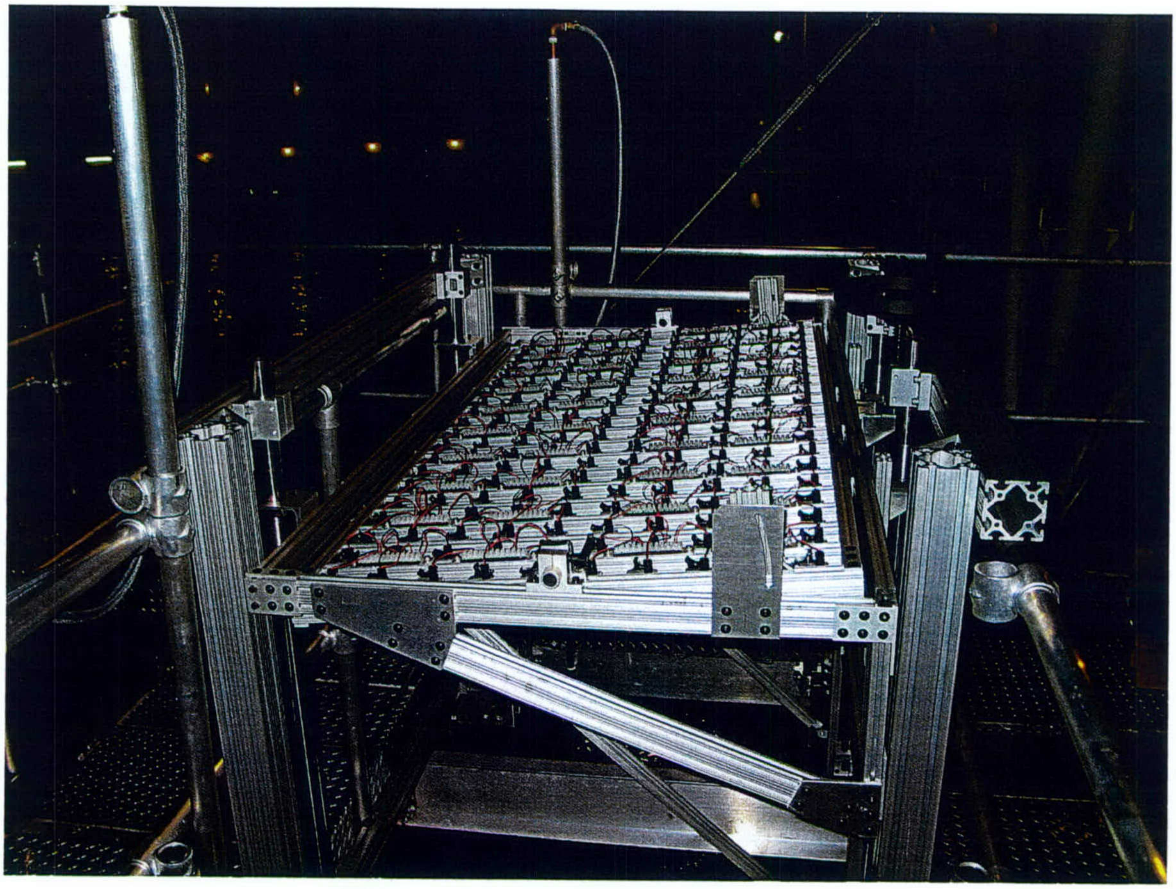

Figure 13: A photograph of a measurement panel in the MASK GLRP system.

UNCERTAINTY ESTIMATE

For the present purpose of performing a general uncertainty analysis, the second-order term in the data reduction equations (2)-(4) will be ignored, so that the relative uncertainties of the physical coordinates of the water surface are reduced to:

$$\frac{U_z}{z_p - a_o} = \frac{U_x}{x_p - b_o} = \frac{U_y}{y_p - c_o} = \frac{U_R}{R} \quad , \tag{5}$$

which states that the relative uncertainty in the physical coordinates is the same as the relative uncertainty in R.

Several factors contribute to the uncertainty associated with the determination of R. The absolute uncertainty of R in pixels will depend on each experimental setup. Estimates are provided in the Table 1 for the Miniature Water Basin demonstration experiment, a typical radio-controlled model (RCM) test, and a typical carriage test. Since the carriage rides along the track under the bridge, mechanical vibration and changing load distribution on the bridge will cause additional uncertainty in R. For all cases, it is assumed that the full scale value of R is set to 100 pixels.

Uncertainty Sources	Miniature Water Basin Test	RCM Test	Carriage Test
Centroid estimation	0.2 pix	0.2 pix	0.2 pix
Optical noise and jitter	0.5 pix	0.5 pix	0.5 pix
Calibration procedure	1.0 pix	1.0 pix	1.0 pix
Vibration	0.2 pix	0.5 pix	1.0 pix
Bridge load distribution	NA	NA	1.0 pix
Total absolute uncertainty	1.2 pix	1.2 pix	1.8 pix
Total relative uncertainty	1.2 %	1.2 %	1.8 %

Table 1: Estimates of overall uncertainty in the GLRP measurement for various experimental setup.

CONCLUSIONS AND FUTURE WORK

The working principle of Global Laser Rangefinder Profilometry, along with its necessary hardware, software, and procedures are explained in detail in this report. GLRP performs cost-effective, spatially distributed measurements at multiple locations over an entire surface. By utilizing multiple laser beams for tagging an array of points on the surface and recording the apparent positions of the laser spots with an area-scan CCD camera, the physical coordinates of the discrete points defining the target surface can be determined through calibration.

An operational GLRP system designed and constructed for model-scale testing at NSWCCD provides high-rate three-dimensional mapping of surface waves over a large physical area in the Maneuvering and Seakeeping Basin. Details of large-amplitude transient wave dynamics in both radio-controlled model (RCM) experiments and carriage tests will lead to better physical understanding and facilitate the development of more sophisticated ship motion prediction and CFD codes by providing data for model development and validation of flow solutions. Even though GLRP is currently designed for model-scale testing, with further development, it is conceivable that the use of GLRP can be extended to full-scale trials for the use of profiling surface waves in the near field of ocean-going vessels.

REFERENCES

1. Jahne, B. and Riemer, K. S., "Two-dimensional wave-number spectra of small-scale water surface waves," Journal of Geophysical Research, **95**, 11531 (1990).

2. Zhang, X., Dabiri, D., and Gharib, M., "Optical mapping of fluid density interfaces: Concepts and implementations,", Review of Scientific Instruments, **67**, 5 (1996).

3. Ciliberto, S. and Gollub, J. P., "Pattern Competition Leads to Chaos," Physical Review Letters, **52**, 922 (1984).

THIS PAGE INTENTIONALLY LEFT BLANK

INITIAL DISTRIBUTION

Copies		Code	Name
3	ONR		
	1	333	Purtell
	1	333	Joslin
	1	334	Kim
3	NAVSEA		
	1		Comstock
	1		Alman
	1		Waters
1	DARPA		
	1		Roesler
2	DTIC		

Center Distribution

Copies	Code	Name
1	002	Corrado
1	3442	Library
1	5010	Koh
1	5030	Jessup
1	5050	Reed
1	5060	Walden
1	5200	Day
1	5200	Cusanelli
1	5200	Hendrix
1	5200	Metcalf
1	5200	Ratcliffe
1	5300	Johnson
1	5300	Coakley

Center Distribution

Copies	Code	Name
1	5300	Furey
1	5300	Irvine
1	5400	Chang
1	5400	Chesnakas
1	5400	Fry
1	5400	Gorski
1	5400	Gowing
1	5400	Miller
1	5400	Park
1	5500	Applebee
1	5500	Belknap
1	5500	Bishop
1	5500	Campbell
1	5500	Dipper
1	5500	Hayden
1	5500	Lin
1	5500	O'Dea
1	5500	Silver
1	5600	Ammeen
1	5600	Bochinski
1	5600	Fu
1	5600	Hess
1	5600	Junghans
1	5600	Sung
1	642	Brizzolara
1	7204	Farabee
1	7410	Smith